U-Pb zircon and Re-Os molybdenite age of the Siah Kamar porphyry molybdenum deposit, NW Iran

Vartan Simmonds[1*], Mohssen Moazzen[2] and David Selby[3,4]

[1] *Research Institute for Fundamental Sciences, University of Tabriz, Tabriz, Iran.*

[2] *Department of Earth Sciences, University of Tabriz, Tabriz, Iran.*

[3] *Department of Earth Sciences, University of Durham, Durham, DH1 3LE, UK*

[4] *State Key Laboratory of Geological Processes and Mineral Resources, School of Earth Resources, China University of Geosciences, Wuhan, 430074, China*

* Corresponding author: Vartan Simmonds
simmonds_vartan@tabrizu.ac.ir

Postal address: 29 Bahman Boulevard, University of Tabriz, Research Institute for Fundamental Sciences,
5166616471, Tabriz–IRAN
Tel: +98-413-3393923
Mobile: +98-9143061461
Fax: +98-413-3250399

Abstract

The Siah Kamar porphyry Mo deposit is the newly discovered deposit of this type in the Neo Tethys-related Urumieh–Dokhtar magmatic arc, northwest Iran. Mineralization occurs as stock-work quartz–molybdenite and mono-mineralic molybdenite veinlets within the porphyry quartz-monzonite stock and the country rocks, accompanied by locally scattered later-stage and cross-cutting quartz-chalcopyrite-pyrite veinlets in the trachy-andesite and trachy-basalt country rocks.

U–Pb zircon geochronology of the porphyry stock yielded Early Oligocene dates of 32.7 ± 0.4 to 30.9 ± 0.4 Ma (at 2σ level). The Th/U ratios of the zircon range between 0.48 and 0.77, and possess initial $\varepsilon Hf_{(t)}$ values of 3.2 to 12.1, which may suggest a dominant mantle source for the magma. Molybdenite separates yielded rhenium contents between ~10 and 41 ppm (average ~26 ppm, n = 4) and slightly younger Re–Os ages compared to the porphyry stock, ranging from 29.1 ± 0.2 to 28.1 ± 0.2 Ma (at 2σ level).

The Siah Kamar porphyry Mo deposit is nearly temporally coeval with the vein-type Cu–Mo–Au mineralization in the Qarachilar and the Haft Cheshmeh porphyry Cu deposit, corresponding to the second porphyry Cu–Mo mineralization epoch in NW Iran. However, it is younger than the majority of the porphyry Cu deposits in the southern Lesser Caucasus, only showing temporal correlation with the Paragachay and first-stage Kadjaran porphyry Cu deposits. Moreover, it is older than all the porphyry Cu–Mo systems across the central and south-eastern parts of the Urumieh–Dokhtar magmatic arc, except the Bondar Hanza deposit, which is nearly coeval with the Siah Kamar porphyry Mo deposit. All these data reveal an old to young trend along the UDMA and the porphyry Cu belt of Iran, further testifying the diachronous and later closure of the Neo-Tethyan oceanic basin in central and SE Iran.

Key words: Siah Kamar, Porphyry Mo, U-Pb zircon dating, Re–Os dating, Hf isotope, Cu–Mo metallogenesis, NW Iran.

1- Introduction

The majority of the well-known porphyry Mo deposits (PMDs) are located in the North America (Westra and Keith 1981; Edwards and Atkinson 1986), though porphyry Mo deposits are also found in Russia, Central Asia (Berzina *et al.* 2005) and China (Westra and Keith 1981; Huang *et al.* 1989; Laznica 2006; Zhu *et al.* 2010). The Siah Kamar PMD is a newly discovered deposit of this type in Iran, which is located 10 km west of Mianeh (NW Iran, Figs. 1 and 2). According to the final exploration report, this deposit contains ore reserves of about 105.6 Mt of which, 39.2 Mt is proven reserves at 539 ppm Mo, and 66.4 Mt is the probable resource at 266 ppm Mo. The ore-host porphyry stock has a quartz-monzonite composition with a relative Oligocene age, which intruded the volcanic and pyroclastic rocks of the Eocene age(Zarnab Ekteshaf 2009; Khaleghi *et al*. 2013).

Based on structural and geologic classifications of Iran, this deposit is situated in the Alborz–Azarbaidjan structural zone (Nabavy 1976) of the Central Iranian Domain (Alavi 1991; Agha Nabaty 2004), on the Cenozoic Urumieh–Dokhtar Magmatic Arc (UDMA) (Fig. 1), which extends from northwest to southeast of Iran over nearly 2000 km and is formed by northeast-ward subduction of the Neo-Tethyan oceanic crust beneath the Central Iranian plate during the Late Mesozoic and Early Cenozoic. The timing of collision, however, is highly controversial (e.g., Agard *et al.* 2011), ranging from Late Cretaceous (Berberian and King 1981) to Miocene (Berberian and Berberian 1981) and even uppermost Pliocene (Stöcklin 1968), with others also suggesting initial collision between the Late Eocene to Oligocene (e.g., Jolivet and Faccenna 2000, Agard *et al.* 2005, Vincent *et al.* 2005, Ballato *et al.* 2010 and references therein).

The UDMA also coincides with the porphyry copper metallogenic belt of Iran, comprised of several metallogenic zones like Ahar–Jolfa (Arasbaran) and Kerman, which host most of the major and small porphyry Cu–Mo deposits (PCDs) and prospects, such as Sungun (NW Iran) and Sarcheshmeh (the largest porphyry deposit; central Iran) (Fig. 1).

This contribution presents the U–Pb age and Hf isotopic composition of zircons from the porphyry stock, as well as the Re abundance within molybdenite samples of the Siah Kamar PMD and their Re–Os age, in order to specify the age of intrusion and mineralization in this deposit. The Hf isotopic composition of zircons can aid in constraining the magma source and the obtained Re concentrations may be used to provide further information regarding the source of parental magma and the physico-chemical characteristics of the ore-forming fluids. Moreover, by comparing the age of this PMD with porphyry Cu–Mo deposits in NW Iran (e.g., Sungun, Haft Cheshmeh, etc.) and the southern Lesser Caucasus (Meghri–Ordubad pluton) (Fig. 2), as well as porphyry mineralizations along the UDMA, such as the Kerman metallogenic zone (Fig. 1), the temporal similarities and differences can be identified and interpreted in order to better constrain the mineralization epochs in the Alborz-Azarbaidjan zone and along the UDMA.

2- Regional geology

The Mianeh–Hashtrood–Bostanabad area (Fig. 2) is mainly distinguished from the neighbouring areas by the occurrence of Cenozoic plutonic rocks. Most of the area is covered by magmatic rocks, as well as Miocene sedimentary units, though Lower Paleozoic to Cretaceous rock units also sporadically crop out in the area. The oldest rock units belong to Cambrian (230 m thick micaceous shale and thin-layered sandstone), which are overlain by Early Cambrian sandstones, Middle–Late Cambrian dolomite and finally, Permian sedimentary units. Outcrops of the Mesozoic rocks are scarce and mainly limited to Late Cretaceous conglomerate, shale and limestone, while the main outcrops of the area are of Eocene, Oligocene and Miocene age. Most of the Eocene units comprise andesite and latite, with intercalations of basaltic, andesitic and dacitic composition.

Post-Eocene magmatism (Oligocene and probably Miocene) is represented by basic–moderate to felsic intrusive bodies emplaced as stocks, domes and dikes, ranging in composition from granodiorite and monzodiorite to granite and porphyritic rhyo-dacite. During the Oligocene, a shallow sedimentary basin was present in the area, which is manifested by the Lower Red Formation of Early Oligocene. This formation is comprised of argillaceous marl with thin-layered intercalations of chalk, shale, red siltstone and sandstone. This environment was later transformed to a marine sedimentary basin during the Miocene. Vast outcrops of Miocene sedimentary units are found within the depressions of the area, including alternations of conglomerate, sandstone, marl and limestone. Emplacement of rhyo-daciticdomes and the deposition of acid tuffs and ignimbrites also occurred in this period. The regression of the Miocene marine environment is highlighted by the Upper Red Formation (Middle–Late Miocene), which is comprised of conglomerate, sandstone and mudstone. Activities of the Sahand volcano commenced in the Late Miocene, covering large areas to the west of the Mianeh–Hashtrood–Bostanabad area and south of Tabriz by lavas and pyroclastic rocks. Volcanic activity of the Sahand continued during the Pliocene and Quaternary, and produced andesitic and dacitic lava flows and pyroclastic rocks. However, contrary to the Ahar–Jolfa zone, no evidence of Late Cretaceous and Plio–Quaternary volcanism was found within this area (Zarnab Ekteshaf 2009).

The occurrence and distribution of hydrothermally altered zones in the Mianeh–Hashtrood–Bostanabad area is far less than in the Ahar–Jolfa (Arasbaran) or Tarom–Hashtjin zones (at the northern and southeast end of this area, respectively) (Fig. 1). However, all these zones encompass similar intrusive bodies and related hydrothermal alterations, which may testify to their similar magmatic and mineralization history (Aria Kansar Samin 2013). Despite the presence of altered zones, only a few mineralized regions have been discovered within the Mianeh–Hashtrood–Bostanabad area. These include native Cu mineralization of Sheikhdar Abad in the west of Mianeh (3 km south of the Siah Kamar PMD), few manganese prospects (e.g., Chay Telor and Zareshlu), as well as kaolinite (Ebek) and gold (Aqveran) deposits (3 and 7 km west of the Siah Kamar PMD, respectively). Evidence of granitoid magmatism and Mo mineralization is found in the Mianeh–Hashtrood area, though it is far less pronounced compared to the Ahar–Jolfa and Tarom–Hashtjin zones, which contain Cu–Mo–Au–Fe and Cu–Pb–Zn–Fe ores, respectively.

2-1 Geology of the Siah Kamar area

Outcropping lithologies in the Siah Kamar area are mainly Eocene volcanic and pyroclastic rocks, which are intruded by Oligocene deep and sub-volcanic intrusive bodies of porphyritic quartz-monzonite and microgranite, as well as andesitic dikes (Fig. 3; Zarnab Ekteshaf 2009).

2-1-1 Eocene volcanic and pyroclastic units

Porphyritic trachy-basalt, basaltic andesite and latite (E^v): The oldest volcanic rocks include alternations of trachy-basalt, basaltic andesite and latite with few intercalations of tuff layers. This complex crops out at the east and north of the study area and is cut by faults with various trends (Fig. 3). This association changes upwards to porphyritic basalts and basaltic andesite lava flows. Some brecciated trachy-andesites are also found in the northwestern margin of the Siah Kamar porphyry stock, adjacent to a fault zone.

Tuff and agglomerate with intercalations of trachy-basaltic to porphyritic basaltic and andesitic lava flows (E^t): This association is stratigraphically found within the lower to middle parts of the E^v unit. Its outcrops are found to the west of the study area (Fig. 3). The main part of the argillic and silicic alterations described in section 4-2 occurs within this association, especially adjacent to the faults and fractures.

2-1-2 Oligocene intrusive and sub-volcanic units

Quartz-monzonite porphyry stock (Qmz): This stock is the oldest intrusive body in the area, which is emplaced into the Eocene volcanic and pyroclastic rocks (Fig. 4a–b) and is cut and dislocated by younger faults. It is dark grey in hand specimen with visible plagioclase phenocrysts. This stock hosts the Mo mineralization and the related hydrothermal alteration, inasmuch as it is intensely altered, especially along the main faults, where some quartz and calcite veins and veinlets are found (Fig. 4c–d).

Porphyritic microgranite (Gr): Outcrops of this rock unit are found to the west of the area (Fig. 3), surrounded by the volcanic and pyroclastic rocks of Eocene (E^t). The color of this unit ranges from yellowish white to cream, red and purple. Argillic and sericitic alterations are dominant. This unit has no contact or cross-cutting evidence with the porphyry stock (Qmz). Its relative age is inferred from its emplacement within the Eocene units and the general geological history of Azarbaidjan region, where post-Eocene intrusive activities belong to Oligocene to Miocene.

Andesitic dikes: Only few andesitic dikes have been found in the northwest of the porphyry stock (Zarnab Ekteshaf 2009). They are about 5 m thick and several hundreds of meters long with NE–SW trend and have intruded the quartz-monzonite stock and the volcanic and pyroclastic rocks (E^v and E^t) and so, they are younger than the porphyry stock and the porphyry molybdenum mineralization.

2-1-3 Pliocene sedimentary units

Post-mineralization Pliocene sedimentary units are found in the southeast of the study area. They include alternations of gypsiferous marl and mudstone with intercalations of conglomerate, sandstone and fresh-water limestone (Pl^m) with thickness of > 100 m, and tens of meters thick alternations of conglomerate with marl, mudstone and fresh-water limestone (Pl^c). The main part of the latter is comprised of conglomerate. The Pl^c unit shows normal contact with Pl^m unit. Both units are not sorted and include clay- to gravel-size grains, as well as gypsum and limestone.

3- Materials and methods

Following field studies and sampling of the rock units in the study area, as well as the diamond-drilled cores, petrographic and mineralogic studies were performed at the Research Institute for Fundamental Sciences, University of Tabriz. Following it, a representative sample from the Siah Kamar porphyry quartz-monzonite stock with potassic alteration (S1 sample, taken from the outcrop near the Qaranqu river; Fig. 3) was chosen for U–Pb zircon dating. Zircons were extracted from the whole-rock using standard techniques of heavy liquid and magnetic separation, and handpicked under a binocular microscope. Then, the zircon grains were sent to the Arizona LaserChron Center (ALC) and were incorporated into a 1" epoxy mount along with multiple fragments of each of ALC 4 primary zircon standards (FC, SL-F, SL-mix, and R33). The mounts were sanded down ~20 microns, polished progressively using a 9, 5, 3, & 1 micron polishing pads, and cathodoluminescence (CL)-imaged using a Hitachi S-3400N scanning electron microscope (SEM) equipped with a Gatan Chroma CL2 detector. Prior to isotopic analysis, the mounts were cleaned in an ultrasound bath of 1% HNO_3 and 1% HCl in order to remove any residual common Pb from the surface of the mount.

Twelve U–Pb analyses were conducted (limited by total number of grains and polished space within the grains) using a 20 micron spot diameter and grain selection and spot placements were based on CL-images, results of which are shown in Supplementary Table 1 (uncertainties in age calculations are at 2σ level). U–Pb geochronology of individual zircon crystals was conducted by laser ablation multicollector inductively coupled mass spectrometry (LA-ICPMS) at the ALC (Gehrels *et al.* 2008). The isotopic analyses involved ablation of zircon using a Photon Machines Analyte G2 excimer laser coupled to a Thermo Element 2 single-collector-ICPMS. Drill rate was ~1 micron/second, resulting in a final ablation pit depth of ~15 microns.

The common Pb correction is accomplished by using the Hg-corrected ^{204}Pb and assuming an initial Pb composition from Stacey and Kramers (1975). Uncertainties of 1.5 for ^{206}Pb/^{204}Pb and 0.3 for ^{207}Pb/^{204}Pb are applied to these compositional values based on the variation in Pb isotopic composition in modern crystalline rocks. Interference of ^{204}Hg with ^{204}Pb is accounted for measurement of ^{202}Hg during laser ablation and subtraction of ^{204}Hg according to the natural ^{202}Hg/^{204}Hg of 4.35.

Hf isotope analyses were conducted with a Nu Plasma MC-ICP-MS connected to a Photon Machines Analyte G2 excimer laser at the Arizona LaserChron Center (ALC). Instrument settings were optimized for laser ablation analyses and seven different standard zircons [Mud Tank (MT), 91500, Temora (TEM), R33, FC52 (FC), Plesovice (PLES), and Sri Lanka (SL or SL-F)] were analyzed. These standards were included with unknowns on the same epoxy mounts. Each standard was analyzed once for every ~15 unknowns. When precision and accuracy were acceptable, unknowns were analyzed using exactly the same acquisition parameters as the standards.

Laser ablation analyses were conducted with a laser beam diameter of 40 microns, with the ablation pits located on top of the U-Pb analysis pits (on the same zircon domains that were previously dated; results are presented in Supplementary Table 2). CL-images were used to ensure that the ablation pits do not overlap multiple age domains or inclusions. Each acquisition consisted of one 40-second integration on backgrounds (on peaks with no laser firing) followed by 60 one-second integrations with the laser firing. Using a typical laser fluence of ~5 J/cm^2 and pulse rate of 7 hz, the ablation rate was ~0.8 microns per second.

Isotope fractionation was accounted for using the method of Woodhead *et al.* (2004): βHf was determined from the measured ^{179}Hf/^{177}Hf; βYb was determined from the measured ^{173}Yb/^{171}Yb (except for very low Yb signals); βLu was assumed to be the same as βYb; and an exponential formula was used for fractionation correction. Yb and Lu interferences were corrected by measurement of ^{176}Yb/^{171}Yb and ^{176}Lu/^{175}Lu (respectively), as advocated by Woodhead *et al.* (2004). Critical isotope ratios were ^{179}Hf/^{177}Hf =0.73250 (Patchett and Tatsumoto 1980); ^{173}Yb/^{171}Yb = 1.132338 (Vervoort *et al.* 2004); ^{176}Yb/^{171}Yb =0.901691 (Vervoort *et al.* 2004; Amelin and Davis 2005); ^{176}Lu/^{175}Lu = 0.02653 (Patchett 1983). All corrections were done line-by-line. For very low Yb signals, βHf was used for fractionation of Yb isotopes. The corrected ^{176}Hf/^{177}Hf values were filtered for outliers (2σ filter), and the average and standard error were calculated from the resulting ~58 integrations. There was no capability to use only a portion of the acquired data.

All solutions, standards, and unknowns analyzed during a session were reduced together. The cutoff for using βHf versus βYb was determined by monitoring the average offset of the standards from their known values, and the cutoff was set at the minimum offset. For most data sets, this was achieved at ~6 mv of ^{171}Yb. For sessions in which the standards yield ^{176}Hf/^{177}Hf values that are shifted consistently from the known values, a correction factor was applied to the ^{176}Hf/^{177}Hf of all standards and unknowns. This correction factor, which was not necessary for most sessions, averaged 1 epsilon unit. The ^{176}Hf/^{177}Hf at time of crystallization was calculated from measurement of present-day ^{176}Hf/^{177}Hf and ^{176}Lu/^{177}Hf, using the decay constant of ^{176}Lu (λ = 1.867e^{-11}) from Scherer *et al.* (2001) and Söderlund *et al.* (2004).

Four molybdenite-bearing samples were selected from diamond-drilled cores within the porphyritic quartz-monzonite stock for Re–Os dating. The locations and depths of the dated samples are noted in Supplementary Table 3. The majority of the molybdenite occurrences in the samples are fine-grained (<2 mm). Pure molybdenite separates were obtained using traditional methods as outlined by Selby and Creaser (2004). An average of 30 mg of pure molybdenite was obtained for each sample. The Re and Os abundance and isotopic composition measurements were conducted on 10 – 20 mg aliquots of molybdenite separates at the University of Durham (UK), as described by Selby and Creaser (2001a, b; Lawley and Selby 2012). As such, given the fine-grained nature of the molybdenite, the analysis of >10 mg significantly reduces probability of Re and Os spatial decoupling (Stein *et al.* 2003; Selby and Creaser 2004). The weighted aliquots of the molybdenite separates and tracer solution (^{185}Re + isotopically normal Os) were loaded into a Carius tube with 11*N* HCl (1 ml) and 15.5*N* HNO_3 (3 ml), sealed and digested at 220°C for ~24 h. Osmium was purified from the acid medium using solvent extraction ($CHCl_3$) at room temperature and micro-distillation methods. The Re fraction was isolated using standard NaOH-acetone solvent extraction and anion column chromatography. The purified Re and Os fractions were loaded onto Ni and Pt wire filaments, respectively, and their isotopic compositions were measured using negative thermal ionization mass spectrometry (Creaser *et al.* 1991; Völkening *et al.* 1991). Analyzes were conducted on a Thermo Scientific TRITON mass spectrometer, with the Re and Os isotope composition measured using static Faraday collection. Full procedural analytical blanks for this study are 2.2 pg for Re and 0.2 pg for Os, with the ^{187}Os/^{188}Os of the blank being 0.28 ± 0.09 (n = 1). Internal uncertainties include uncertainties related to Re and Os mass spectrometer measurements, blank abundances and isotopic compositions, and spike calibrations. The reproducibility of the isotopic measurements was checked using RM8599 NIST molybdenite standard, which was analyzed during the same period as that of Li *et al.* (2017b,c). The Re–Os ages obtained for the RM8599 are 27.69 ± 0.04, which is in good agreement with the recommended value 27.66 ± 0.10 Ma (Markey *et al.* 2007; Zimmerman *et al.* 2014), and previous analysis at Durham (Lawley and Selby 2012).

The model Re–Os ages for molybdenites (t) were calculated by assuming no initial ^{187}Os, similar to the method of McCandless *et al.* (1993) and using the following equation:

$$(1)\, t = \frac{1}{\lambda}\ln(1 + {}^{187}Os/{}^{187}Re)$$

where λ is the decay constant of ^{187}Re ($1.666\times10^{-11} \pm 0.017$ a^{-1}; Smoliar *et al.* 1996).The uncertainties for the model ages are reported as the 2σ absolute level in two forms; full analytical + tracer, and full analytical + tracer + decay constant uncertainties (given in brackets) (Supplementary Table 3).

4- Background information on the Siah Kamar deposit

4-1 Petrography of the quartz-monzonite porphyry stock

According to the petrographic studies and the geochemical data and classification provided by Khaleghi *et al.* (2013), the porphyry stock has quartz-monzonite composition and contains plagioclase phenocrysts set in a fine to medium-grained groundmass comprised of plagioclase, K-feldspar and quartz (Fig. 5a–b) portraying a porphyritic texture. Plagioclase (40 – 50 %) occurs as mostly fresh fine microlites, as well as euhedral to subhedral phenocrysts (< 5 mm) with Carlsbad and occasionally polysynthetic twinning.

K-feldspar (20 – 35 %) and quartz (10 – 20 %) occur as anhedral fine to medium grains within the groundmass. Quartz is locally found as medium-sized anhedral grains and moreover, silicic veinlets are also found within the porphyry stock. Opaque minerals (<5 %) are found as anhedral to subhedral grains disseminated within the groundmass, as well as within the quartz veinlets or occur as mono-mineralic veinlets. Based on mineralographic studies, most of the disseminations within the host porphyry stock are magnetite, though pyrite is also present, with relatively larger and more euhedral grains. The abundance of opaque minerals within the sericitic alteration zone reaches up to 10 %. Primary ferro-magnesian minerals were not recognized within the studied samples, but fine flakes of secondary biotite are commonly observed within the groundmass (0 – 10 %), showing a considerable increase towards the potassic alteration zone. Apatite and zircon form the accessory minerals.

4-2 Geochemistry and petrogenesis of the Siah Kamar porphyry stock

Based on the geochemical analysis data (n = 11; Khaleghi *et al.* 2013), the porphyry stock has a relatively high silica (60.6–73.3 wt%, with an average of 65.7 wt%), K_2O+Na_2O (7.4–11.5 wt%) and Al_2O_3 (14.2–19.79 wt%) and low TiO_2 (0.28–0.6 wt%), MgO (0.1–1.27 wt %) and CaO (0.37–2.30 wt%) contents.

Considering the geochemical composition of the fresh samples of the porphyry stock and the criteria defined by Westra and Keith (1981) for the Climax-type vs. Endako-type (quart monzonite-type) PMDs, especially the Rb (71–250 ppm with the average of 173 ppm; <250 ppm), F (<3%), Nb (15–23 ppm with the mean of 19 ppm; <20 ppm), Ta (0.73–2.37 with the average of 1.1 ppm; almost <2 ppm,) and Sr (212–958 ppm with the mean of 536 ppm; >100 ppm) concentrations, as well as the distribution of the alteration zones (Fig. 3), the Siah Kamar deposit is classified as an Endako-type PMD. Most of the samples show high-K calc-alkaline and shoshonitic characteristics and mainly peraluminous composition. Trace element-based discrimination diagrams show a post-collisional volcanic arc setting for the studied intrusive body. In addition, chondrite-normalized distribution pattern of the trace and rare earth elements display enrichment of LIL elements and depletion of HFSEs, which is in agreement with subduction related magmatism (Khaleghi *et al.* 2013).

4-3 Hydrothermal alteration

Hydrothermal alteration zones have been developed within the host porphyry stock and the country rocks, with more intense occurrence in the vicinity of faults and the intrusive stock. Hydrothermal alteration includes potassic, sericitic, silicic, argillic and propylitic assemblages, which show a regular zonation from the center of the porphyry stock towards the country rocks.

According to field investigations and diamond-drilled cores, the potassic alteration is mainly developed within the central part of the porphyry stock and even it has affected the adjacent volcanic rocks in contact with the porphyry stock. This alteration zone contains the main part of the molybdenite mineralization and is characterized by the formation of large amounts of secondary biotite within the groundmass (sometimes up to 40 %), as well as disseminated magnetite (Fig. 5c). Moreover, stockwork-type veinlets of quartz + molybdenite + magnetite (±orthoclase) are also distinguished in this zone. Secondary biotite aggregates give a mottled appearance to the porphyry stock in this zone.In the deeper levels, the potassic alteration zone is much more extensive in the northern outcrop of the porphyry stock (north of the Qaranqu river; Fig. 3), where it is surrounded by the sericitic alteration zone. The boundary between these two zones is transitional, where the sericitic alteration is superimposed on the potassic zone. Finally, both zones are surrounded by propylitic alteration zone. However, in the southern part of the stock, the potassic alteration has a transitional boundary with the propylitic alteration zone.

Sericitic alteration occurs both within the porphyry stock and the adjacent volcanic and pyroclastic rocks. The most considerable feature of this zone is the moderate to intense sericitization of feldspars, inasmuch as the sericite content reaches up to 50 % and due to it, this alteration is introduced as sericitic. Other minerals formed in this zone are secondary quartz, pyrite, chlorite and Fe oxides–hydroxides (Fig. 5d). The latter two minerals are products of the supergene alteration. Furthermore, stock-work veinlets containing quartz, sericite and pyrite are present within this zone, along with Fe-oxide veinlets (<1 cm thick), which most likely were initially pyrite-bearing.

Silicic alteration has mainly occurred within the central part of the region and accompanies the potassic alteration, as well as within the tuffs and agglomerates of the Eocene age (E^t). Moreover, quartz veinlets have also been formed within the porphyry stock, especially in its central part of the stock, within the potassic alteration zone, as well as within the volcanic country rocks. Their thickness ranges from mm scale up to several cm (<10 cm) and they display stockwork texture. These veinlets are locally cross-cut by calcite veinlets (<1 cm). Additionally, 23 silicic veins are discovered in the area, which have various trends ranging from N–S to NE–SW and occasionally NW–SE (Aria Kansar Samin Co. 2013).

The argillic alteration is observed in the northern outcrop of the porphyry stock and the peripheral volcanic–pyroclastic rocks. The intensity of this alteration is weak to moderate. This zone is especially found in the vicinity of fault zones and is occasionally accompanied by silicic veinlets. Based on XRD analysis results (Zarnab Ekteshaf 2009), the main minerals are montmorillonite, kaolinite, quartz and sericite.

Propylitic alteration is the most extensive hydrothermal alteration zone, which is mainly developed in the northern part of the porphyry stock and has also affected the Eocene volcanic rocks. The mineral assemblage characterizing this alteration zone includes chlorite, epidote, calcite, actinolite and tremolite, which have replaced feldspars and ferro-magnesian minerals and to lesser extent, occur as veinlets. This alteration zone overprints the potassic alteration zone at the southern part of the porphyry stock.

4-4 Hypogene mineralization

Based on the current investigation, as well as previous studies of Zarnab Ekteshaf (2009), Aria Kansar Samin (2013) and Khaleghi *et al.* (2013), molybdenum mineralization occurs mainly within the porphyry quartz-monzonite stock, and subordinately within the Eocene volcanic rocks to the north, with an overall length of about 1 km and width of 300–500 m. The ore-bearing trachy-andesitic country rock at the vicinity of the porphyry stock is about 500 m long and 250 m wide. Diamond drillings within the mineralized zone reveal that Mo mineralization is present to a depth of 600 m.

Molybdenite (from trace amounts up to 0.5 vol.%) is disseminated within the host quartz-monzonite, the stockwork-type quartz and quartz–K feldspar veinlets and/or mono-mineralic molybdenite veinlets of several cm (<10 cm) to <1 cm thick, especially in the potassic alteration zone (Fig. 6a). It is also found as open-space fillings within the porphyry stock. Magnetite (< 5 vol.%) is found as anhedral aggregates (Fig. 6 b–c), as well as disseminations within the porphyry stock, especially in the potassic alteration zone, and shows weak martitization.

In addition to it, a later stage Cu mineralization is also locally and sporadically found within the trachy-andesite and trachy-basalt country rocks, extending in an area of several decametres. This mineralization is mainly restricted to the fractured zones and appears as veinlets (<1 cm thick) or open-space fillings and is accompanied by weak to moderate calcic and argillic alterations. According to the geochemical data provided by Zarnab Ekteshaf (2009), the highest Cu content among 10 ICP-MS analyses are 0.26% and 0.21%, obtained from an andesitic dike and the trachy-basaltic country rock, respectively. Other data for Cu in the porphyry stock and the country rocks range between 7 and 61 ppm (average of 27.3 ppm).The Cu content in a sample from the potassic alteration zone is about 58 ppm.

The later stage quartz-sulfide veinlets contain pyrite, chalcopyrite, along with trace amounts of bornite, covellite and hematite. They cross-cut the quartz-molybdenite veinlets, causing clear dislocation along them. Pyrite (0 – 1 vol.%) occurs as large to fine euhedral to subhedral grains within the open-space fillings, as well as within the quartz–sulfide veinlets. Chalcopyrite (< 0.3 vol.%) occurs as inclusions surrounded within the pyrite grains (Fig. 6b–c). Evidence of supergene sulfide enrichment in the form of replacement by covellite and bornite is observed at the margins of these inclusions (Fig. 6c). Finally, late-stage barren quartz and calcite veinlets cross-cut the earlier generations and the country rocks (<1 cm).

According to the results of 87 surficial samples taken from the porphyry stock and the altered country rock (analyzed by AAS method in the laboratory of Sarcheshmeh Cu Complex; Khaleghi *et al.* 2013), the average Mo grade is above 0.02 %, with a maximum value of 0.27 %. However, subsurface core samples reveal grades up to 0.54% with an average of 0.25 %. In addition to molybdenite, W accompanies Mo in the potassic zone (max.= 30.6 ppm), as well as within the trachy-basaltic country rock (max.= 16.3 ppm), though most of the W data fall within the range of 3.2 and <0.5 ppm. Weak mineralization of gold is also evident; the highest Au content is obtained from quartz veinlets (303 ppb) and the microgranitic intrusive body (130 ppb). Silicic and argillic alteration zones show weak enrichment of gold, while other samples contain negligible amounts of Au (1–55 ppb, mean= 11.34 ppb from) (Zarnab Ekteshaf 2009; Aria Kansar Samin 2013).

Regarding the mineralization in the Siah Kamar area, since the porphyry stock only hosts molybdenite with no concomitant Cu-sulfide mineralization, and by considering the fact that the only occurrences of Cu is in the trachy-andesite and trachy-basalt country rocks, where the quartz-chalcopyrite-pyrite veinlets cross-cut and postdate the quartz-molybdenite veinlets, the Siah Kamar deposit has been introduced as porphyry molybdenite deposit.

5- Results

5-1 U–Pb ages and Hf isotopic composition of the analyzed zircons

Twelve spots on the separated zircons were analyzed for U-Pb dating. Zircons are 150-250 μm long, predominantly euhedral and prismatic, with aspect ratios of 2 to 3 and concentric oscillatory zoning of magmatic origin. No inherited cores were detected. The analytical data are reported in Supplementary Table 1. One analysis (spot 46) was deleted during data reduction due to relatively high uranium concentration compared to the rest of the sample. One other analysis (spot 49) was rejected due to low concordance. The resulting interpreted ages of ten analyzed zircons are shown on the Pb*/U concordia and weighted mean diagrams using the routines in Isoplot (Ludwig 2008; Fig., 7), the obtained ^{206}Pb/^{238}U ages of which range from 32.70 ± 0.40 Ma to 30.90 ± 0.40 Ma (Supplementary Table 1) with a weighted mean age of 31.41± 0.37 Ma (at 2σ level) (MSWD=0.0113; Fig. 7) corresponding to Early Oligocene age (Rupelian). Meanwhile, the U and Th contents of the analyzed zircons are 689 – 314 and 149.5 – 530 ppm, respectively, with averages of 413.5 and 266 ppm, respectively. On this basis, the Th/U ratio of the analyzed zircons ranges between 0.48 and 0.77 (Fig. 8a), indicating a magmatic source for the zircons (Teipel *et al.* 2004).

Six laser-ablation Lu-Hf measurements were performed on the dated zircon grains. The Supplementary Table 2 summarizes the Hf isotope data obtained from zircons. The analyzed zircons have ^{176}Lu/^{177}Hf ratios of 0.000976-0.002557 and present day ^{176}Hf/^{177}Hf ratios between 0.282856 and 0.283118, with positive initial $\varepsilon Hf_{(t)}$ values (at the time of zircon crystallization) of 3.2 to 12.1, which are distributed between the CHUR (Chondritic Uniform Reservoir model; Blichert-Toft and Albarède 1997) and the Depleted Mantle evolution (DM; Griffin *et al.* 2000) lines (Fig. 8b). $\varepsilon Hf_{(t)}$values indicate a rather inhomogeneous source, making reconciling them with derivation from a single magma difficult. Higher $\varepsilon Hf_{(t)}$ variations may show zircons crystallization from a magma undergoing continuous assimilation-fractional crystallization or the interaction of the magma from the depleted mantle source with the crustal lithospheric materials. This variation cannot be accounted for different magmas with different ages (e.g. Griffin *et al.* 2000), since all show very similar U-Pb ages. Single-stage depleted-mantle model ages (T_{DM}) were calculated using the measured ^{176}Lu/^{177}Hf ratios, referred to a model depleted mantle with a present-day ^{176}Hf/ ^{177}Hf = 0.28325, similar to that of average MORB (Nowell *et al.* 1998) and ^{176}Lu/^{177}Hf = 0.0384 (Griffin *et al.* 2000); this is similar, though not identical, to the depleted mantle curve defined by juvenile rocks through time (Vervoort and Blichert-Toft, 1999). These T_{DM} ages represent a minimum age for the source material of the host magma from which the zircon crystallized, which range from 197 to 564 Ma for the studied samples (Supplementary Table 2). We also present the more realistic two-stage Hf model ages (T_{DM}^{C}) of the source rocks for the magmas, derived by projecting the initial $^{176}Hf/^{177}Hf$ of the zircon back to the depleted mantle model growth curve, assuming a mean crustal value for Lu/Hf ($^{176}Lu/^{177}Hf = 0.015$; Griffin *et al.* 2002). The T_{DM}^{C} ages for the analyzed zircons are about 284 – 875 Ma (Supplementary Table 2).

5-2 Re content and Re–Os age of molybdenites

The Re concentration in the four representative molybdenite separates collected from molybdenite-bearing veinlets within the porphyry stock (Supplementary Table 3) are between ~10 and 41 ppm, with an average concentration of 25.8 ± 13 ppm (1 SD, n = 4). The ^{187}Os abundance ranges from ~3.1 – 12.2 ppb, with an average of 7.7 ± 3.8 ppb (Supplementary Table 3). The calculated model ages range between 29.06 ± 0.20 [0.22] (sample K2 – bracketed uncertainties includes the uncertainties in the decay constant) and 28.10 ± 0.15[0.18] Ma (sample K3) (Fig. 9). The Re-Os dates for samples K1 and K3 are broadly identical including uncertainty (28.28 ± 0.13[0.16] and 28.10 ± 0.15[0.18] Ma, respectively). Considering that the Re-Os ages do not overlap with uncertainties, it may be suggested that mineralization occurred episodically in this PMD (e.g., Stein 2014, Li *et al.* 2017a,b).

6- Discussion

6-1 Re content interpretation for molybdenites

At the first glance and by a simple comparison, the rhenium content of the studied molybdenites corresponds to the Re range of molybdenites in global porphyry Mo deposits, which is about tens of ppm (e.g., Berzina *et al.* 2005) and differs from those of porphyry Cu and Cu–Mo deposits, which have higher Re contents about hundreds of ppm. This difference can primarily be related to the volume dilution of Re with the presence of high molybdenite content in porphyry Mo deposits, whereas in Cu–dominated deposits the Re content of the co-existing scarce molybdenites will be increased (Stein *et al.* 2001a; Berzina *et al.* 2005). However, many other variables such as temperature, pH, *f*Cl, magma source, etc. can affect the Re content of molybdenites (Selby *et al.* 2001), discussion of which is out of the aim of this contribution. The measured Re contents are in the range of most of the measured PMDs in Russia and Central Asia, as well as the typical deposits of Endako in Canada, Climax and Urad Henderson in the USA. The average Re content of the studied samples is a little lower than the average of 42 ppm calculated based on 19 PMDs and porphyry Mo–Cu deposits across the world (Berzina *et al.* 2005). This can be resulted from relatively lower *f*Cl conceived from the very low population of halite and sylvite-bearing fluid inclusions within the ore-bearing quartz veinlets, which may have negative impact on the Re transportation by ore-bearing fluids (availability of Re) and its precipitation within the molybdenites.

On a regional scale of northwest and central Iran, as well as the southern Lesser Caucasus, the Siah Kamar deposit is the only PMD discovered so far and so, there is no other counterpart to make comparison. When comparing it with porphyry Cu–Mo deposits across the region, it is clearly seen that the measured values for the Siah Kamar PMD are much lower than those of PCDs, which can simply and dominantly be attributed to the volume dilution of Re at the presence of high molybdenite content in the PMDs.

6-2 U–Pb and Re–Os age data and temporal interpretations

The zircon U–Pb ages for the Siah Kamar quartz-monzonite porphyry stock indicate that its crystallization occurred during 32.7 ± 0.4 to 30.9 ± 0.4 Ma, corresponding to the Early Oligocene (Rupelian).

The molybdenite model Re-Os ages for the Siah Kamar PMD indicate that mineralization based on the sample set occurred, in part, between 29.06 ± 0.20[0.22] and 28.10 ± 0.15[0.18] Ma (bracketed uncertainties include the uncertainty in the decay constant), constraining the timing of mineralization to the Middle

Oligocene (upper part of the Rupelian). Further, the Re-Os molybdenite dates, including all uncertainties, suggest that Mo mineralization at Siah Kamar occurred over a minimum and maximum duration of 0.56 and 1.35 Ma, respectively. Meanwhile, comparing the ages of crystallization and mineralization obtained in this study for the Siah Kamar ore deposit, it can be said that mineralization has started at least ~1.5 Ma after the emplacement and crystallization of the porphyry stock (Fig. 10). However, it must be noted that considerable uncertainties remain in estimating this time interval (Li *et al.* 2017b).

Given that no other PMDs have been discovered in Iran or in the southern Lesser Caucasus to date, it is not possible to make any conclusion regarding the age constraints of PMDs in these regions. However, comparing the ages of crystallization and mineralization in the Siah Kamar PMD with dominantly distributed PCDs in Iran reveals the temporal relationship between these two types of mineralization. As discussed earlier, porphyry Cu–Mo mineralization in Iran is present predominantly along the UDMA, including the Ahar–Jolfa, Central Iran and Kerman Cu metallogenic zones, as well as in the east Iran (Fig. 1). The PCDs of east Iran are the oldest deposits, dated to the Late Eocene (~37 – 39 Ma; Aghazadeh *et al.* 2015) and are related to the closure of the Sistan oceanic basin between the Lut and Afghan blocks. The Siah Kamar PMD is younger than these PCDs. The second oldest metallogenic zone is the Ahar–Jolfa zone in northwest Iran, which includes the nation's second largest PCD of Sungun, as well as several other smaller PCDs and prospects. Taking into account the published ages for the PCDs and prospects in Ahar–Jolfa zone, Simmonds *et al.* (2017) have proposed three epochs of porphyry Cu mineralization in this area, including Late Eocene (represented by Saheb Divan PCD), Middle Oligocene (including the Haft Cheshmeh PCD and the vein-type Cu–Mo–Au mineralization in the Qarachilar area, for which some authors speculate about porphyry-type genesis) and the Early Miocene (e.g., Sungun, Masjed Daghi, Kighal and Niaz PCDs and prospects) (Fig. 2). Comparing the ages obtained for the Siah Kamar PMD with the PCDs in the Ahar–Jolfa zone reveals that mineralization in the Siah Kamar corresponds to the second porphyry mineralization epoch in the Ahar–Jolfa zone, being more or less coeval with the Haft Cheshmeh PCD and showing a narrow temporal overlap with the Cu–Mo–Au mineralization of Qarachilar.

Given that the Ahar–Jolfa zone shares many magmatic, geodynamic and mineralization features with the neighboring South Armenian Block (SAB) of the southern Lesser Caucasus and that the Meghri–Ordubad pluton is considered the northern extension of the Qaradagh batholith in NW Iran (Fig. 2), the ages of porphyry Cu and Mo deposits in both areas may help to better understand the magmatic and mineralization activities in the whole region. Compared to the Cenozoic metallogenic evolution of the SAB proposed by Moritz *et al.* (2016b) and Rezeau *et al.* (2016), the Siah Kamar deposit fits with the second Cenozoic event dated as Oligocene, similar to the PCDs in northwest Iran. The Siah Kamar deposit is nearly coeval with the Paragachay and the first stage of mineralization in the world-class Kadjaran PCDs, although postdates most of the PCDs in SAB, especially those of the Late Eocene age (Fig. 2). The only younger event is the second stage of mineralization in the Kadjaran PCD, dating at 20.48 ± 0.1 Ma (molybdenite Re–Os age), as well as Cu-rich epithermal veins overprinting porphyritic granodioritic dikes (dated at 22.2 ± 0.30 Ma) (Rezeau *et al.* 2016).

Finally, intrusion and mineralization in the Siah Kamar deposit is older than all the porphyry Cu–Mo mineralizations across the central and SE parts of the UDMA, except the Bondar Hanza PCD in the Kerman zone (Fig. 1) with the U–Pb age of 30.20 ± 0.90to 26.60 ± 0.80 (mean of 27.35 ± 0.71) and the Re–Os age of 28.71 ± 0.46 to 28.06 ± 0.47 Ma (Aghazadeh *et al.* 2015), which nearly correlate with the ages of Siah Kamar PMD. Other dated PCDs and prospects in this zone range between 16.19± 0.23 Ma (Chah Firouzeh PCD) and 6.19 ± 0.10 Ma (Abdar PCD; Aghazadeh *et al.* 2015) (Fig. 1), showing ages of Lower to Middle Miocene.

7- Conclusion

The Siah Kamar porphyry Mo deposit is the first porphyry molybdenum deposit discovered in the UDMA. The Re abundance of molybdenite separates is comparable with global porphyry Mo deposits (e.g., Climax and Henderson in the USA), being clearly distinguished from porphyry Cu–Mo deposits, which typically possess several hundred ppm Re. The relatively high Re content of the Siah Kamar molybdenites, compared to the global average of PMDs, may be attributed to a mixed mantle+crust source for supplying the ore materials, with the dominance of mantle component, which is also supported by the positive initial $\varepsilon Hf_{(t)}$ values and the Th/U ratios of zircons from the porphyry stock.

The U–Pb dating of the zircons from the quartz-monzonite porphyry stock in the Siah Kamar PMD yielded ages of 32.7 ± 0.4 Ma to 30.9 ± 0.4 Ma, corresponding to an Early Oligocene age. The Re–Os dating of molybdenites from the Siah Kamar PMD indicates that mineralization occurred episodically between 29.06 ± 0.22 to 28.10 ± 0.18 Ma, which corresponds to the Middle Oligocene (upper part of the Rupelian). These two data sets testify that mineralization has potentially occurred ~1.5 Ma after the crystallization of the porphyry stock, though the uncertainties remain in this regard. Comparing the ages obtained for molybdenites of the Siah Kamar with porphyry Cu–Mo mineralizations in the southern Lesser Caucasus indicates that this deposit is younger than many of the dated PCDs and prospects in the Meghri–Ordubad pluton, especially those of the Late Eocene, although it is roughly coeval with the Paragachay and the first-stage mineralization in Kadjaran PCDs (Fig. 10).

On the regional scale of NW Iran, mineralization in the Siah Kamar corresponds to the second porphyry mineralization epoch in NW Iran, proposed by Simmonds *et al.* (2017), showing an overlap or similar ages with the Haft Cheshmeh PCD and the vein-type Cu–Mo–Au mineralizations in the Qaradagh batholith (Fig. 10). The age of the Siah Kamar porphyry stock is also coeval with the calc-alkaline magmatism in the Shaivar Dagh intrusive complex with the zircon U-Pb age of 30.8 ±2.1 Ma (Aghazadeh *et al.* 2011).

In contrast, mineralization in the Siah Kamar is older than all the porphyry Cu–Mo mineralizations across the central and southeastern parts of the UDMA, except the Bondar Hanza PCD in the Kerman zone, which nearly correlates with the Siah Kamar PMD (Fig. 10). All these comparisons signify the migration of the magmatic activities and the related mineralizations along the UDMA following the collision between the Arabian and Iranian plates, which was earlier in NW Iran and occurred later in SE Iran (e.g., Agard *et al.* 2011).

Acknowledgements

This study was financially supported by the Deputy Dean of the Research Bureau of University of Tabriz through the grant No. 6814. Authors would like to express their appreciation to the authorities in this bureau. DS acknowledges the Total Endowment Fund and the Dida Scholarship of CUG, Wuhan. Thanks are also extended to Prof. R. Moritz and Prof. G. Topuz and other unknown reviewers, whose constructive comments and suggestions helped to improve the manuscript, as well as Dr. Jamal Honar Pajouh and Hiva Nik Khah for their cooperation in field work and sample preparation.

References

Agard, P., Omrani, J., Jolivet, L., and Mouthereau, F., 2005, Convergence history across Zagros (Iran): constraints from collisional and earlier deformation: International Journal of Earth Sciences (Geologische Rundschau), v. 94, p. 401–419.

Agard, P., Omrani, J., Jolivet, L., Whitechurch, H., Vrielynck, B., Spakman, W., Monie, P., Meyer, B., and Wortel, R., 2011, Zagros Orogeny: a subduction-dominated process: Geological Magazine, v. 148, p. 692-725.

Agha Nabaty, E., 2004, Geology of Iran: Tehran, Geological survey and mineral exploration organization of Iran, 586 p. (in Persian).

Aghazadeh, M., Castro, A., Badrzadeh, Z., and Vogt, K., 2011, Post-collisional polycyclic plutonism from the Zagros hinterland: the Shaivar Dagh plutonic complex, Alborz belt, Iran: Geological Magazine, v. 148, p. 980–1008.

Aghazadeh, M., Castro, A., Rashidnejad Omran, N., Emami, M.H., Moinvaziri, H., and Badrzadeh, Z., 2010, The gabbro (shoshonitic)–monzonite–granodiorite association of Khankandi pluton, Alborz Mountains, NW Iran: Journal of Asian Earth Sciences, v. 38, p. 199–219.

Aghazadeh, M., Hou, Z., Badrzadeh, Z., and Zhou, L., 2015, Temporal–spatial distribution and tectonic setting of porphyry copper deposits in Iran: constraints from zircon U–Pb and molybdenite Re–Os geochronology: Ore Geology Reviews, v. 70, p. 385–406.

Alavi, M., 1991, Sedimentary and structural characteristics of the Paleo-Tethys remnants in northeastern Iran: Geological Society of America Bulletin, v. 103, p. 983–992.

Amelin, Y., and Davis, W.J., 2005, Geochemical test for branching decay of ^{176}Lu: Geochimica et Cosmochimica Acta, v. 69, p. 465–473.

Aminzadeh, B., Shahabpour, J., and Maghami, M., 2011. Variation of rhenium contents in molybdenites from the Sar Cheshmeh Cu-Mo deposit in Iran: Resource Geology, v. 61, p. 290–295.

Aria Kansar Samin Co., 2013, 1:1000 geologic map and alteration report of the Siah Kamar area. Final exploration report of the Siah Kamar area: Tabriz, East Azarbaidjan Province Industry, Mine and Trade Organization, 67 pp.

Bahlburg, H., Vervoort, J.D., and DuFrane, S.A., 2010, Plate tectonic significance of Middle Cambrian and Ordovician siliciclastic rocks of the Bavarian facies, Armorican terrane assemblage, Germany: U–Pb and Hf isotope evidence from detrital zircons: Gondwana Research, v. 17, p. 223–235.

Ballato, P., Mulch, A., Landgraf, A., Strecker, M.R., Dalconi, M.C., Friedrich, A., and Tabatabaei, S.H., 2010, Middle to late Miocene Middle Eastern climate from stable oxygen and carbon isotope data, southern Alborz mountains, N Iran: Earth and Planetary Science Letters, v. 300, p. 125–138.

Berberian, M., 1983, The southern Caspian: A compressional depression floored by a trapped, modified oceanic crust, Canadian Journal of Earth Sciences, v. 20, p. 163–183.

Berberian, F., and Berberian, M., 1981, Tectono-plutonic episodes in Iran, *In* Gupta, H.K., and Delany, F.M., eds., Zagros-Hindu Kush-Himalaya Geodynamic Evolution: American Geophysical Union, v. 3, p. 5–32.

Berberian, M., and King, G.C.P., 1981, Towards a paleogeography and tectonic evolution of Iran: Canadian Journal of Earth Sciences, v. 18, p. 210–265.

Berzina, A.N., Sotnikov, V.I., Economou-Eliopoulos, M., and Eliopoulos, D.G., 2005, Distribution of rhenium in molybdenite from porphyry Cu–Mo and Mo–Cu deposits of Russia (Siberia) and Mongolia: Ore Geology Reviews, v. 26, p. 91–113.

Blichert-Toft, J., and Albarede, F., 1997, The Lu-Hf isotope systematic of garnet pyroxinites from Beni Bousera, Morocco: implications for basalt origin: Contributions to Mineralogy and Petrology, v. 127, p. 248–260.

Creaser, R.A., Papanastassiou, D.A., and Wasserburg, G.J., 1991, Negative thermal ion mass spectrometry of osmium, rhenium and iridium: Geochimica et Cosmochimica Acta, v. 55, p. 397–401.

Edwards, R., and Atkinson, K., 1986, Ore deposit geology, and its influence on mineral exploration: London, Chapman and Hall, 466 p.

Filimonova, L.Y., Zhukov, N.M., and Malyavka, A.G., 1984, Genetic aspects of polytypism and rhenium contents of molybdenite in porphyry copper deposits: Geochimiya, v. 7, p. 1040–1046 (in Russian).

Gehrels, G.E., Valencia, V., Ruiz, J., 2008, Enhanced precision, accuracy, efficiency and spatial resolution of U–Pb ages by laser ablation-multicollector-inductively coupled plasma-mass spectrometry: Geochemistry, Geophysics, Geosystems, v. 9, Q03017, doi:10.1029/2007GC001805.

Griffin, W.L., Pearson, N.J., Belousova, E., Jackson, S.E., van Achterbergh, E., O’Reilly, S.Y., and Shee, S.R., 2000, The Hf isotope composition of cratonic mantle: LAM-MC-ICPMS analysis of zircon megacrysts in kimberlites: Geochimica et Cosmochimica Acta, v. 64, p. 133–147.

Griffin, W.L., Wang, X., Jackson, S.E., Pearson, N.J., O'Reilly, S.Y., Xu, X., and Zhou, X., 2002, Zircons chemistry and magma genesis in SE China: in situ analysis of Hf isotopes, Pingtan and Tonglu igneous complexes: Lithos, v. 61, p. 237–269.

Hassanpour, S., 2010, Cu–Au metallogenesis and mineralization in Arasbaran zone (East Azarbaidjan, Iran) [Ph.D. thesis]: Tehran, Shahid Beheshti University, 330 p. (in Persian).

Hassanpour, S., Alirezaei, S., Selby, D., and Sergeev, S., 2015, SHRIMP zircon U–Pb and biotite and hornblende Ar–Ar geochronology of Sungun, Haftcheshmeh, Kighal, and Niaz porphyry Cu–Mo systems: evidence for an early Miocene porphyry-style mineralization in northwest Iran: International Journal of Earth Sciences, v. 104, p. 45–59.

Huang, D., Dong, Q., and Gan, Zh., 1989, China Molybdenum Deposits. Beijing, Geological Publishing House, p. 482–538.

Jolivet, L., and Faccenna, C., 2000, Mediterranean extension and the Africa-Eurasia collision: Tectonics, v. 19, p. 1095–106.

Khaleghi, F., Hosseinzadeh, Gh., Rasa, I., and Moayyed, M., 2013, Geological and geochemical characteristics of the Siah Kamar porphyry molybdenum deposit, west of Mianeh, NW Iran: Geosciences, v. 22, p. 187–196 (in Persian with English abstract).

Lawley, C.J.M., and Selby, D., 2012, Re–Os geochronology of quartz enclosed ultra-fine molybdenite: implications for ore geochemistry: Economic Geology, v. 107, p. 1499–1506.

Laznica, P., 2006, Giant Metallic Deposits: Berlin, Springer publishing, p. 180–200.

Li, Y., Li, X. H., Selby, D., and Li, J. W., 2017a, Pulsed magmatic fluid release for the formation of porphyry deposits: tracing fluid evolution in absolute-time from the Tibetan Qulong Cu-Mo deposit: Geology, v. 46, p. 7-11.

Li, Y., Selby, D., Condon, D., and Tapster, S., 2017b, Cyclic Magmatic-Hydrothermal Evolution in Porphyry Systems: High-Precision U-Pb and Re-Os Geochronology Constraints on the Tibetan Qulong Porphyry Cu-Mo Deposit: Economic Geology, v. 112, p. 1419-1440.

Li, Y., Selby, D., Feely, M., Costanzo, A., and Li, X. H., 2017c, Fluid inclusion characteristics and molybdenite Re-Os geochronology of the Qulong porphyry copper-molybdenum deposit, Tibet: Mineralium Deposita, v. 52, p. 137-158.

Ludwig, K., 2008, Isoplot 3.6: Berkeley Geochronology Center Special Publication 4, 77 pp.

Magakian, I.G., Amiryan, Sh.O, Zaryan, R.N., and Karamyan, K.A., 1984, Minerals of ore formations of Armenian SSR, vol. 1. Yerevan, Publishing House of Armenian SSR, 306 p. (in Russian).

Markey, R., Stein, H.J., Hannah, J.L., Zimmerman, A., Selby, D., and Creaser, R.A., 2007, Standardizing Re-Os geochronology: a new molybdenite Reference Material (Henderson, USA) and the stoichiometry of Os salts: Chemical Geology, v. 244, p. 74–87.

McCandless, T.E., Ruiz, J., and Campbell, A.R., 1993, Rhenium behaviour in molybdenite in hypogene and near-surface environments: implications for Re–Os geochronology: Geochimica et Cosmochimica Acta, v. 57, p. 889–905.

Moritz, R., Melkonyan, R., Selby, D., Popkhadze, N., Gugushvili, V., Tayan, R., Ramazanov, V., 2016a, Metallogeny of the Lesser Caucasus: From arc construction to post-collision evolution. *In* Richards, J., ed., Tethyan tectonics and metallogeny: Special Publication of the Society of Economic Geology, v. 19, p. 157–192.

Moritz, R., Rezeau, H., Ovtcharova, M., Tayan, R., Melkonyan, R., Hovakimyan, S., Ramazanov, V., Selby, D., Ulianov, A., Chiaradia, M., and Putlitz, B., 2016b, Long-lived, stationary magmatism and pulsed porphyry systems during Tethyan subduction to post-collision evolution in the southernmost Lesser Caucasus, Armenia and Nakhitchevan: Gondwana Research, v. 37, p. 465–503.

Nabavy, H., 1976, An introduction to the geology of Iran: Tehran, Geological Survey of Iran, 109 p. (in Persian).

Nowell, G.M., Kempton, P.D., Noble, S.R., Fitton, J.G., Saunders, A.D., Mahoney, J.J., and Taylor, R.N., 1998, High precision Hf isotope measurements of MORB and OIB by thermal ionisation mass spectrometry: insights into the depleted mantle: Chemical Geology, v. 149, p. 211–233.

Patchett, P.J., 1983, Importance of the Lu–Hf isotopic system in studies of planetary chronology and chemical evolution: Geochimica and Cosmochimica Acta, v. 47, p. 81–91.

Patchett, P.J., and Tatsumoto, M., 1980, A routine high-precision method for Lu–Hf isotope geochemistry and chronology: Contributions to Mineralogy and Petrology, v. 75, 263-267.

Rezeau, H., Moritz, R., Wotzlaw, J.F., Tayan, R., Melkonyan, R., Ulianov, A., Selby, D., d'Abzac F.X., and Stern, R.A., 2016, Temporal and genetic link between incremental pluton assembly and pulsed porphyry Cu-Mo formation in accretionary orogens: Geology, v. 44, p. 627–630.

Scherer, E., Münker, C., and Mezger, K., 2001, Calibration of the Lutetium-Hafnium Clock: Science, v. 293, p. 683–687.

Selby, D., and Creaser, R.A., 2001a, Re–Os geochronology and systematics in molybdenite from the Endako porphyry molybdenum deposit, British Columbia, Canada: Economic Geology, v. 96, p. 197–204.

Selby, D., and Creaser, R.A., 2001b, Late and Mid-Cretaceous mineralization in the Northern Canadian Cordillera: constraints from Re–Os molybdenite dates: Economic Geology, v. 96, p. 1461–1467.

Selby, D., and Creaser, R.A., 2004, Macroscale NTIMS and microscale La-MC-ICP-MS Re–Os isotopic analysis of molybdenite: Testing spatial restrictions for reliable Re–Os age determinations, and implications for the decoupling of Re and Os within molybdenite: Geochimica et Cosmochimica Acta, v. 68, p. 3897–3908.

Simmonds, V., and Moazzen, M., 2015, Re–Os dating of molybdenites from Oligocene Cu–Mo–Au mineralized veins in the Qarachilar area, Qaradagh batholith (northwest Iran): implications for understanding Cenozoic mineralization in South Armenia, Nakhchivan and Iran: International Geology Review, v. 57, p. 290–304.

Simmonds, V., Moazzen, M., and Mathur, R., 2017, Constraining the timing of porphyry mineralization in NW Iran in relation to Lesser Caucasus and Central Iran; Re–Os age data for Sungun porphyry Cu-Mo deposit: International Geology Review, in press.

Smoliar, M.I., Walker, R.J., and Morgan, J.W., 1996, Re–Os ages of Group IIA, IIIA, IVA, and IVB iron meteorites: Science, v. 271, p. 1099–1102.

Söderlund, U., Patchett, P.J., Vervoort, J.D., and Isachsen, C.E., 2004, The ^{176}Lu decay constant determined by Lu–Hf and U–Pb isotope systematics of Precambrian mafic intrusions: Earth and Planetary Science Letters, v. 219, p. 311–324.

Stacey, J.S., and Kramers, J.D., 1975, Approximation of terrestrial lead isotope evolution by a two-stage model: Earth and Planetary Science Letters, v. 26, p. 207–221.

Stein, H.J., 2014. Dating and Tracing the History of Ore Formation, in Turekian, H.D.H.K., ed., Treatise on Geochemistry, 2nd ed.: Oxford, Elsevier, p. 87–118.

Stein, H. J., Markey, R. J., Morgan, J. W., Hannah J. L. and Schersten, A., 2001, The remarkable Re–Os chronometer in molybdenite: how and why it works: Terra Nova, v. 13, p. 479–486.

Stein, H.J., Schersten, A., Hannah, J., and Markey, R., 2003, Subgrain-scale decoupling of Re and ^{187}Os and assessment of laser ablation ICP-MS spot dating in molybdenite: Geochimica et Cosmochimica Acta, v. 67, p. 3673–3686.

Stöcklin, J., 1968, Structural history and tectonics of Iran: a review, American Association of Petroleum Geologists Bulletin, v. 52, p. 1229–1258.

Teipel, U., Eichhorn, R., Loth, G., Rohrmüller, J., Höll, R., and Kennedy, A., 2004, U–Pb SHRIMP and Nd isotopic data from the western Bohemian Massif (Bayerischer Wald, Germany): implications for Upper Vendian and Lower Ordovician magmatism: International Journal of Earth Sciences, v. 93, p. 782–801.

Topuz, G., Candan, O., Zack, T., Yilmaz, A., 2017, East Anatolian plateau constructed over a continental basement: No evidence for the East Anatolian accretionary complex, Geology, v. 45, p. 791–794.

Vervoort, J.D., 2010, Hf analysis in zircon by LA-MC-ICPMS: Promise and pitfalls: Geological Society of America Abstracts with Programs, v. 42, p. 667.

Vervoort, J.D., and Blichert-Toft, J., 1999, Evolution of the depleted mantle: Hf isotope evidence from juvenile rocks through time: Geochimica et Cosmochimica Acta, v. 63, p. 533–556.

Vervoort, J.D., Patchett, P.J., Söderlund, U., and Baker, M., 2004, The isotopic composition of Yb and the precise and accurate determination of Lu concentrations and Lu/Hf ratios by isotope dilution using MC-ICPMS: Geochemistry, Geophysics, Geosystems, v. 4, Q1102, DOI 2004GC000721RR.

Vincent, S.J., Allen, M.B., Ismail-Zadeh, A.D., Flecker, R., Foland, K.A., and Simmons, M.D., 2005, Insights from the Talysh of Azerbaijan into the Paleogene evolution of the South Caspian region, Geological Society of America Bulletin, v. 117, p. 1513–1533.

Völkening, J., Walczyk, T., and Heumann, K.G., 1991, Osmium isotope ratio determinations by negative thermal ionization mass spectrometry: International Journal of Mass Spectrometry and Ion Processes, v. 105, p. 147–159.

Westra, G., and Keith, S.B., 1981, Classification and genesis of stockwork molybdenum deposits: Economic Geology, v. 76, p. 844–873.

Whitney, D.L., and Evans, B.W., 2010, Abbreviations for names of rock-forming minerals: American Mineralogist, v. 95, p. 185–187.

Wieser, M.E., 2006, Atomic weights of the elements 2005 (IUPAC Technical Report): Pure and Applied Chemistry, v. 78, p. 2051–2066.

Woodhead, J., Hergt, J., Shelley, M., Eggins, S., and Kemp, R., 2004, Zircon Hf-isotope analysis with an excimer laser, depth profiling, ablation of complex geometries, and concomitant age estimation: Chemical Geology, v. 209, p. 121–135.

Zarnab Ekteshaf Consultant Engineers, 2009, Geologic and alteration studies in Siah Kamar area in 1:25000 scale: Tehran, Iranian National Cupper Industries Company, 97 p (in Persian).

Zhu, L., Zhang, G., Guo, B., Lee, B., and Wang, F., 2010, Geochemistry of the Jinduicheng Mo- bearing porphyry and deposit, and its implications for the geodynamic setting in East Qinling, P. R. China: Chemie der Erde, v. 70, p. 159–174.

Figure Captions

Fig. 1 The main tectonic zones of Iran (Agha Nabaty 2004), the Cu metallogenic zones with some major and minor porphyry Cu deposits (1. Sungun, 2. Chah Firouzeh, 3. Abdar, 4. Sarcheshmeh, 5. Bondar Hanza, 6. Maher Abad) and the location of the study area. The Urumieh–Dokhtar magmatic arc (UDMA) includes the NW–SE trending Cenozoic volcanic and plutonic rocks, parallel to the Neo-Tethyan suture zone. The Alborz and Sistan sutures are from Berberian (1983), the Sevan–Akra suture is from Moritz *et al.* (2016a) and the Zagros suture is from Agard *et al.* (2011) and Topuz *et al.* (2017). Outline of the Fig. 2 is shown in NW Iran. AAZ=Alborz–Azarbaidjan zone (Nabavy, 1976).

Fig. 2 Distribution of the Cenozoic (mainly Oligo–Miocene) granitoids in NW Iran and South Armenia, including the major Meghri–Ordubad and Qaradagh plutons and other smaller intrusives, along with the location of the Ahar–Jolfa metallogenic zone and the Mianeh–Hashtrood–Bostanabad area, as well as the main porphyry Cu–Mo, base and precious metal deposits in the region. Presented ages are from Moritz *et al.* (2016 a and b) and Rezeau *et al.* (2016) for Dastakert, Hankasar, Kadjaran, Paragachay and Agarak (Re-Os), Hassanpour (2010) for Saheb Divan (^{40}Ar/^{39}Ar), Aghazadeh *et al.* (2015) for Haft Cheshmeh and Masjed Daghi (Re-Os), Hassanpour *et al.* (2015) for Niaz (^{40}Ar/^{39}Ar), Aghazadeh *et al.* (2011) for Shaivar Dagh (zircon U-Pb), Simmonds and Moazzen (2015) for Qarachilar (Re-Os), Simmonds *et al.* (2017) for Sungun (Re-Os), and unpublished zircon U-Pb data from the first author for Kighal. Outline of the Fig. 3 is shown by dotted line in NW Iran.

Fig. 3 1:25000 geologic and alteration map of the Siah Kamar area (simplified and modified after Zarnab Ekteshaf 2009 and Aria Kansar Samin Co. 2013).

Fig. 4 Field photographs of the Siah Kamar PMD. (a) The northern and (b) the southern outcrops of the Siah Kamar porphyry stock (looking northwest and south, respectively), (c) quartz veinlets within the porphyry stock, (d) sericitic alteration zone within the porphyry stock.

Fig. 5 Photomicrographs illustrating the Siah Kamar porphyry stock and the hydrothermal alteration zones within it. (a) and (b) Plagioclase phenocrysts set in a fine-grained groundmass made of quartz and feldspar, (c) potassic alteration characterized by the formation of fine flakes of secondary biotite, (d) intense sericitic alteration. Mineral abbreviations from Whitney and Evans (2010).

Fig. 6 Photomicrographs of ore minerals in the Siah Kamar PMD. (a) first-stage mineralization: molybdenite mainly occurs as veinlets within the porphyry stock, (b) later-stage mineralization: anhedral and brecciated pyrite with chalcopyrite inclusions, accompanied by anhedral magnetite, (c) replacement of chalcopyrite inclusions by covellite in the supergene enriched zone. Mineral abbreviations from Whitney and Evans (2010).

Fig. 7(a) U–Pb concordia diagram for zircons from the Siah-Kamar porphyry stock. (b) Weighted mean diagram of the ages obtained for the analyzed zircons.

Fig. 8 (a) Th and U concentrations in the analyzed zircons from the Siah Kamar porphyry stock. Relevant Th/U ratios are included for comparison: 1.0 = lower limit for magmatic zircon from mafic rocks, 0.3-0.4 = accepted lower limits for magmatic zircon and 0.1 = upper limit for metamorphic zircon (Teipel *et al.* 2004).The available data of other porphyry stocks and volcanic rocks from the UDMA and NW Iran are also shown for comparison (Aghazadeh et al., 2010 for Khankandi; Hassanpour et al. 2015 for Sungun and Haft Cheshmeh). (b) T–εHf plot for the analyzed zircons from the Siah Kamar porphyry stock. Reference lines representing the chondrite Hf evolution (CHUR; Blichert-Toft and Albarède 1997) and the depleted mantle (DM; Griffin *et al.* 2000). The Depleted-Mantle model ages (T_{DM}) are also shown.

Fig. 9 Re-Os ages of molybdenites from the Siah Kamar PMD (uncertainties at 2σ absolute level).

Fig. 10 Schematic illustration of zircon U-Pb ages of the intrusive rocks (red boxes) and Re-Os ages of molybdenite (gray boxes) for the Siah Kamar PMD and the almost coeval magmatic and mineralization events in SAB, NW and central parts of the UDMA (including the entire analytical errors). Presented ages are from Moritz *et al.* (2016 a and b) and Rezeau *et al.* (2016) for Kadjaran and Paragachay, Aghazadeh *et al.* (2015) for Haft Cheshmeh and Bondar Hanza, Aghazadeh *et al.* (2011) for Shaivar Dagh, and Simmonds and Moazzen (2015) for Qarachilar.

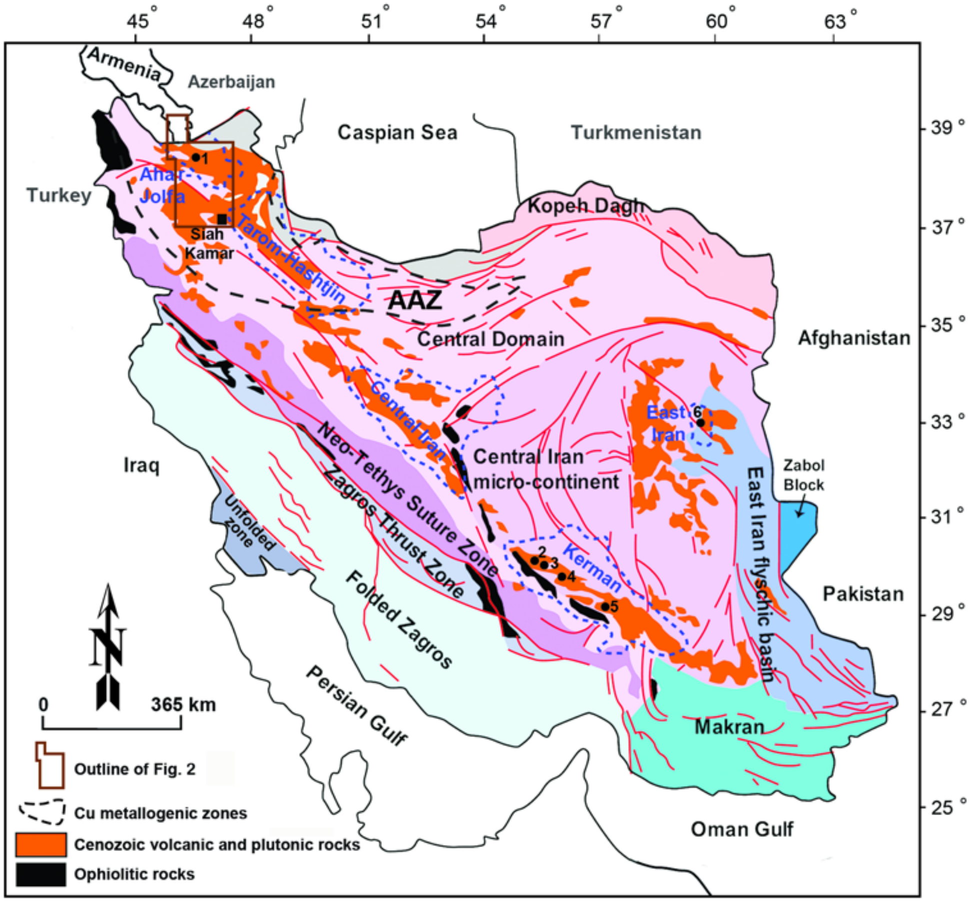
45°
48°
51°
54°
57°
60°
63°
39°
37°
35°
33°
31°
29°
27°
25°
Armenia
Azerbaijan
Caspian Sea
Turkmenistan
Turkey
Kopeh Dagh
Ahar-Jolfa
1
Siah Kamar
Tarom-Hashtjin
AAZ
Central Domain
Afghanistan
Central Iran
East Iran
6
Central Iran micro-continent
Iraq
Zabol Block
Neo-Tethys Suture Zone
Zagros Thrust Zone
Unfolded Zone
East Iran flyschic basin
Kerman
2
3
4
5
Pakistan
Folded Zagros
N
0
365 km
Persian Gulf
Makran
Oman Gulf
Outline of Fig. 2
Cu metallogenic zones
Cenozoic volcanic and plutonic rocks
Ophiolitic rocks

Fig. 1

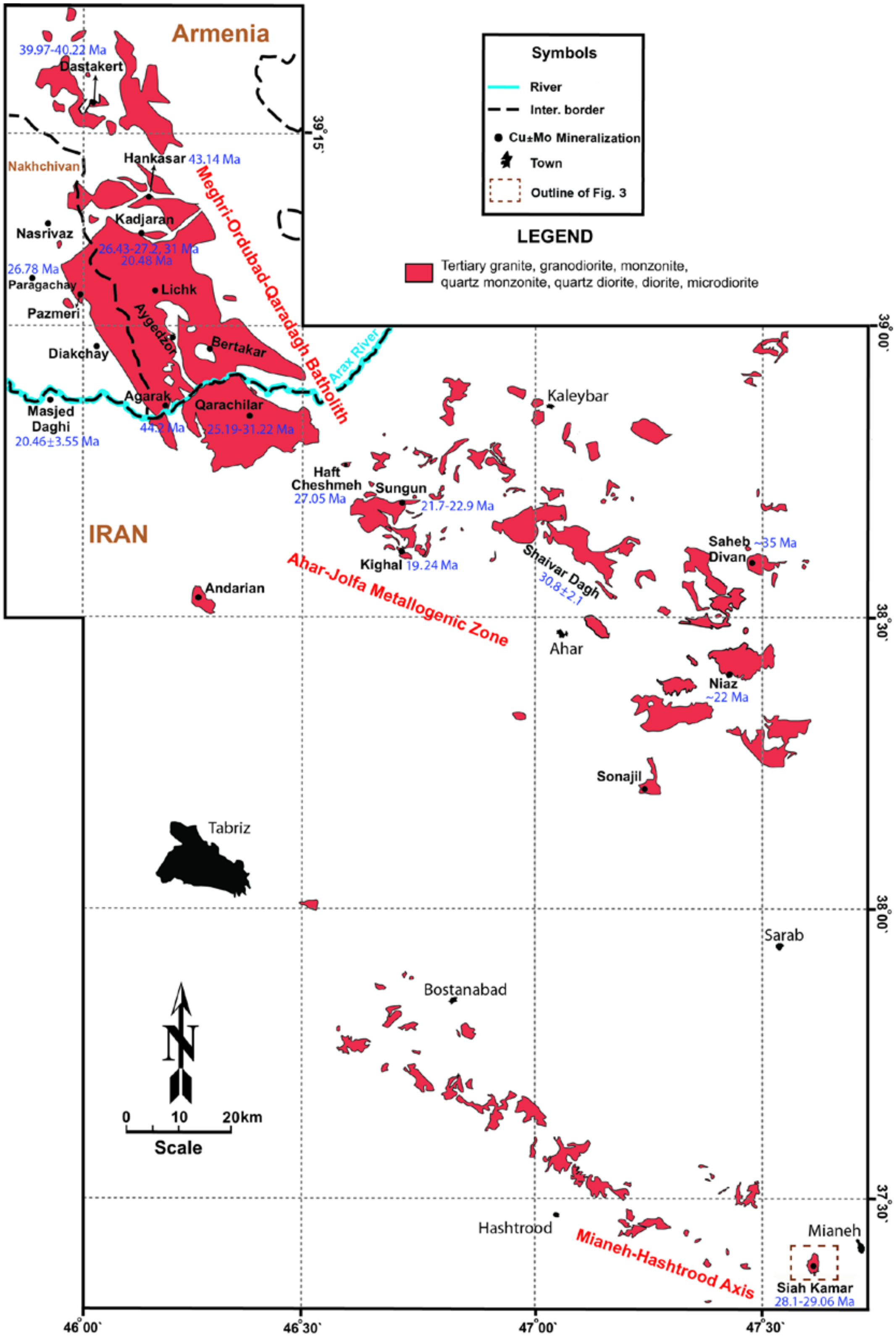
Armenia
39.97-40.22 Ma
Dastakert
39°15`
Nakhchivan
Hankasar 43.14 Ma
Meghri-Ordubad-Qaradagh Batholith
Kadjaran
Nasrivaz
26.43-27.2, 31 Ma
20.48 Ma
26.78 Ma
Paragachay
Lichk
Pazmeri
Aygedzor
Diakchay
Bertakar
Arax River
Agarak
Qarachilar
Masjed Daghi
20.46±3.55 Ma
44.2 Ma
25.19-31.22 Ma
IRAN
Symbols
River
Inter. border
● Cu±Mo Mineralization
Town
Outline of Fig. 3
LEGEND
Tertiary granite, granodiorite, monzonite, quartz monzonite, quartz diorite, diorite, microdiorite
39°00`
Kaleybar
Haft Cheshmeh
27.05 Ma
Sungun
21.7-22.9 Ma
Kighal 19.24 Ma
Saheb Divan ~35 Ma
Shaivar Dagh
30.8±2.1
Andarian
Ahar-Jolfa Metallogenic Zone
38°30`
Ahar
Niaz
~22 Ma
Sonajil
Tabriz
38°00`
Sarab
Bostanabad
N
0
10
20km
Scale
37°30`
Hashtrood
Mianeh
Mianeh-Hashtrood Axis
Siah Kamar
28.1-29.06 Ma
46°00`
46°30`
47°00`
47°30`

Fig. 2

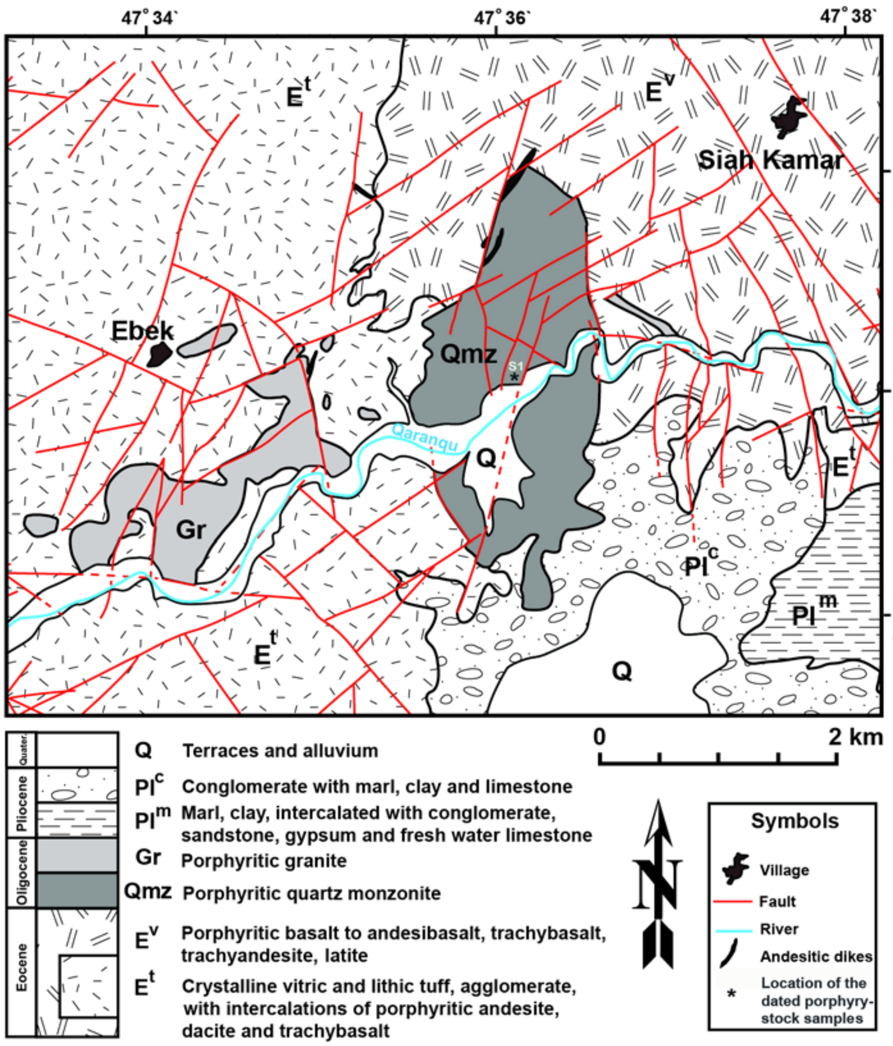
47° 34`
47° 36`
47° 38`
37° 25`
37° 24`
37° 23`
E^t
E^v
Siah Kamar
Ebek
Qmz
S1
Qarangu
Q
Gr
E^t
Pl^c
Pl^m
E^t
Q
0
2 km
Quater.
Pliocene
Oligocene
Eocene
Q Terraces and alluvium
Pl^c Conglomerate with marl, clay and limestone
Pl^m Marl, clay, intercalated with conglomerate, sandstone, gypsum and fresh water limestone
Gr Porphyritic granite
Qmz Porphyritic quartz monzonite
E^v Porphyritic basalt to andesibasalt, trachybasalt, trachyandesite, latite
E^t Crystalline vitric and lithic tuff, agglomerate, with intercalations of porphyritic andesite, dacite and trachybasalt
N
Symbols
Village
Fault
River
Andesitic dikes
* Location of the dated porphyry-stock samples

Fig. 3

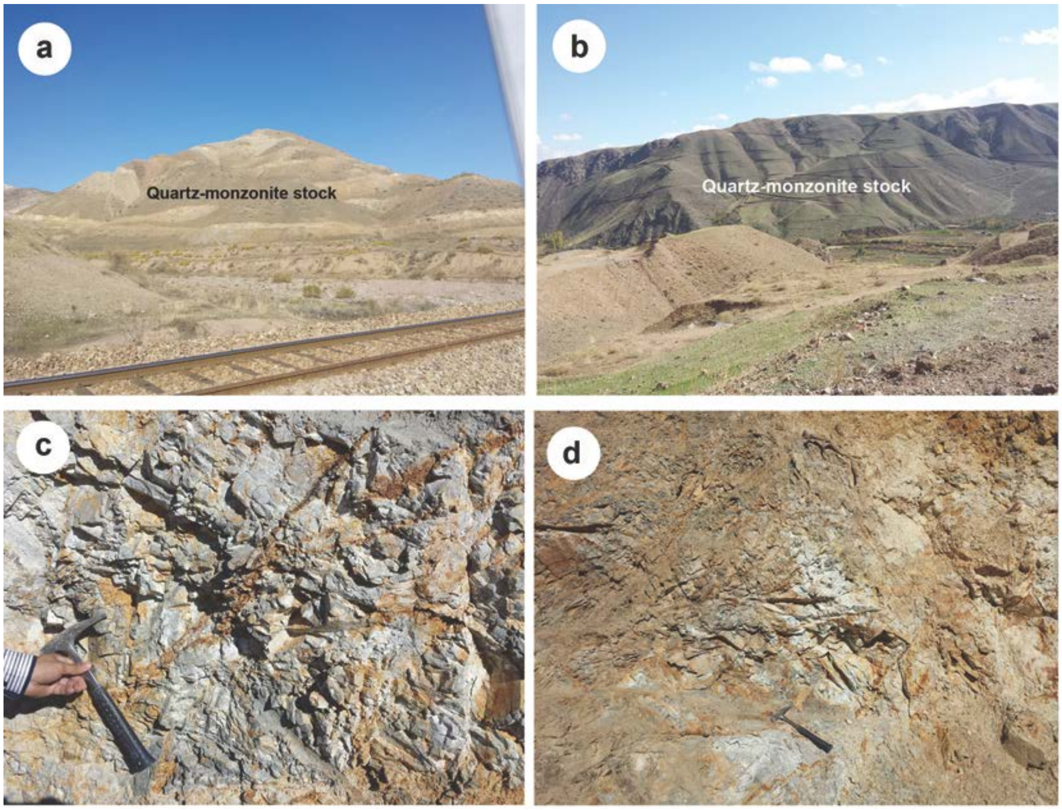

Fig. 4

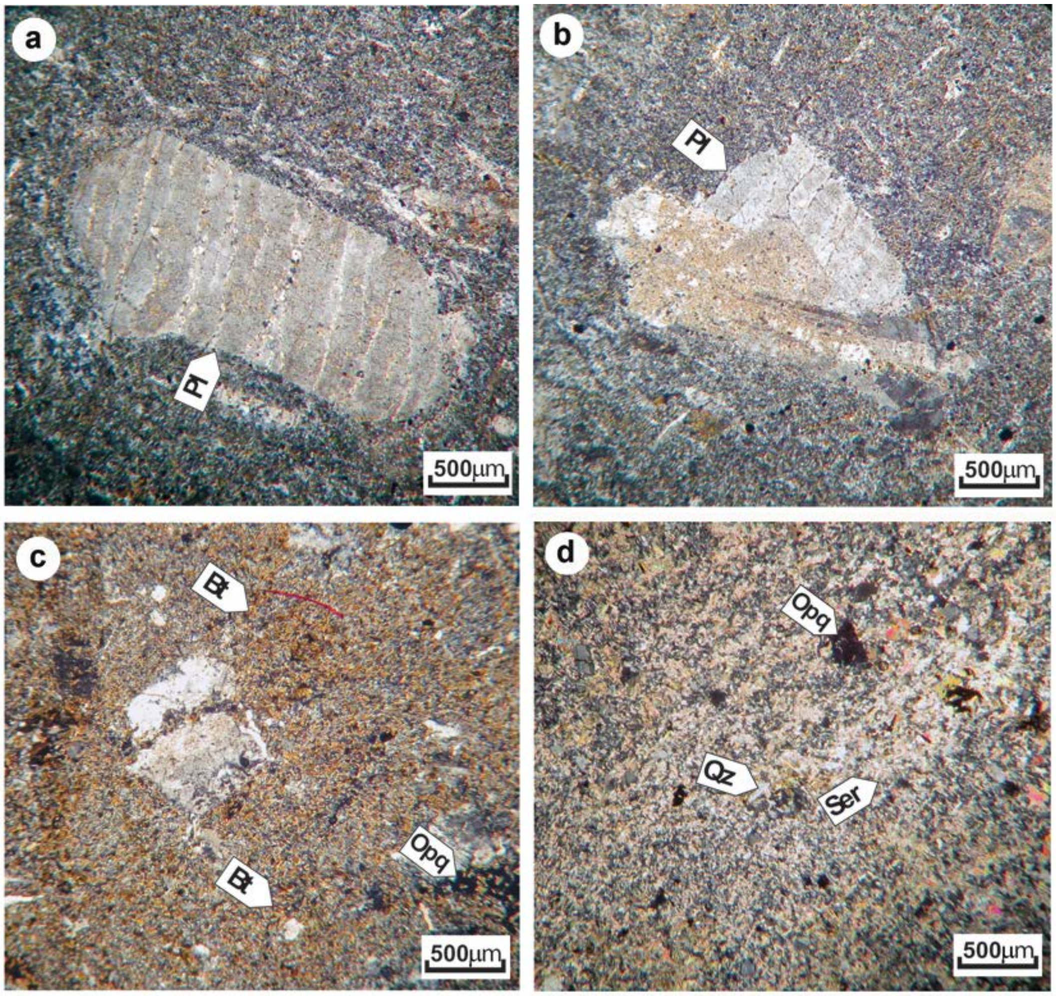

Fig. 5

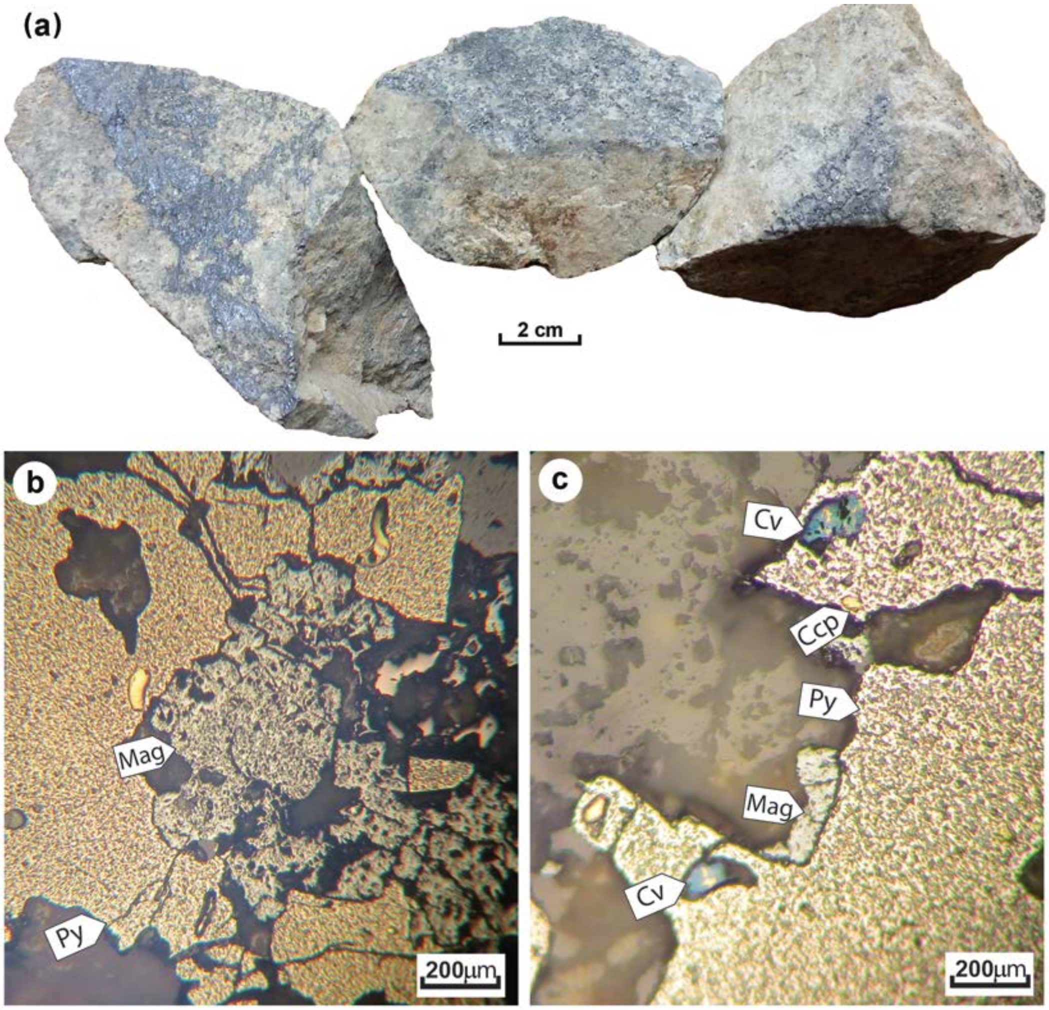
(a)
2 cm
b
Mag
Py
200μm
c
Cv
Ccp
Py
Mag
Cv
200μm

Fig. 6

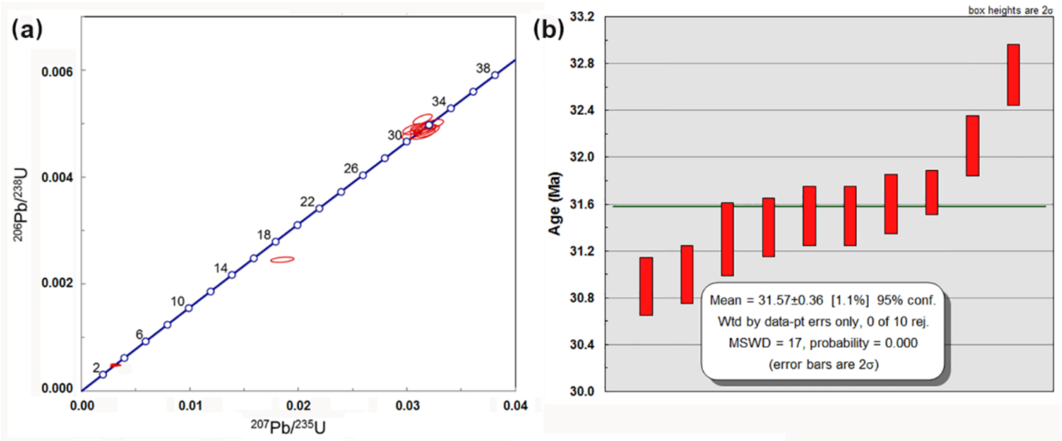
(a)
$^{206}Pb/^{238}U$
$^{207}Pb/^{235}U$
0.000
0.002
0.004
0.006
0.00
0.01
0.02
0.03
0.04
2
6
10
14
18
22
26
30
34
38
(b)
box heights are 2σ
Age (Ma)
33.2
32.8
32.4
32.0
31.6
31.2
30.8
30.4
30.0
Mean = 31.57±0.36 [1.1%] 95% conf.
Wtd by data-pt errs only, 0 of 10 rej.
MSWD = 17, probability = 0.000
(error bars are 2σ)

Fig. 7

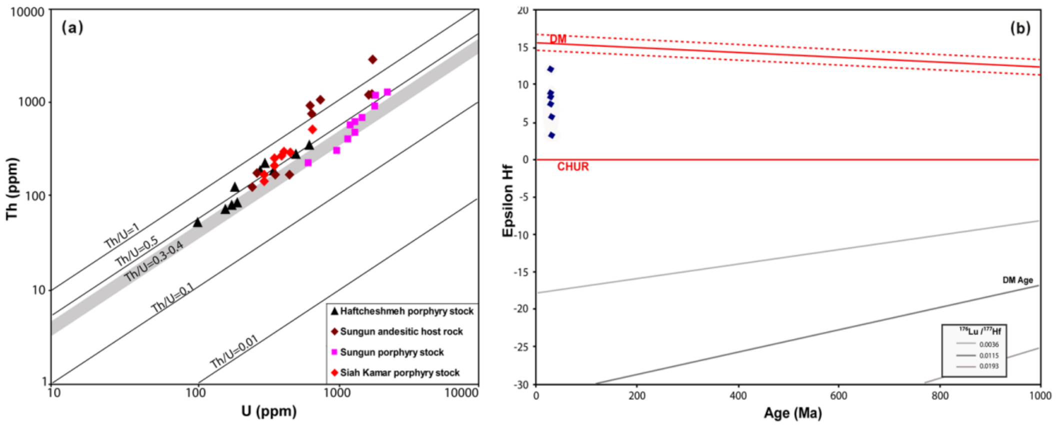
(a)
Th (ppm)
10000
1000
100
10
1
U (ppm)
10
100
1000
10000
Th/U=1
Th/U=0.5
Th/U=0.3-0.4
Th/U=0.1
Th/U=0.01
▲ Haftcheshmeh porphyry stock
◆ Sungun andesitic host rock
■ Sungun porphyry stock
◆ Siah Kamar porphyry stock
(b)
Epsilon Hf
20
15
10
5
0
-5
-10
-15
-20
-25
-30
DM
CHUR
DM Age
$^{176}Lu/^{177}Hf$
0.0036
0.0115
0.0193
Age (Ma)
0
200
400
600
800
1000

Fig. 8

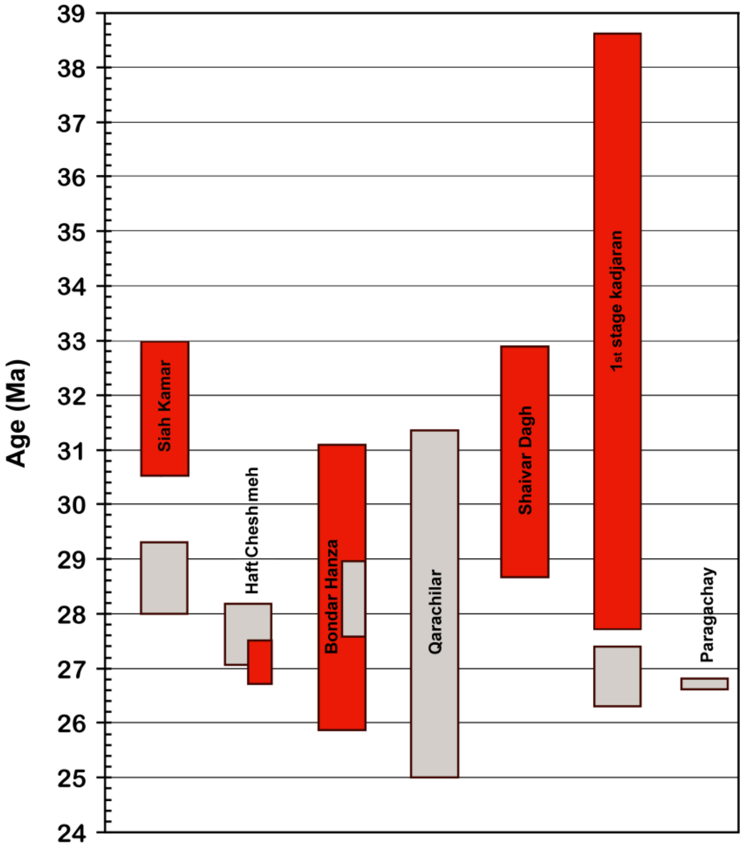
Age (Ma)
39
38
37
36
35
34
33
32
31
30
29
28
27
26
25
24
Siah Kamar
Haft Cheshmeh
Bondar Hanza
Qarachilar
Shaivar Dagh
1st stage kadjaran
Paragachay

Fig. 9